MASONRY INFILL WALLS UNDER BLAST LOADING USING CONFINED UNDERWATER BLAST WAVE GENERATORS (WBWG)

João M. Pereira [a]*, José Campos [b], Paulo B. Lourenço [a]

[a] ISISE, Department of Civil Engineering, University of Minho, Guimarães, Portugal

[b] Department of Mechanical Engineering, University of Coimbra, Coimbra, Portugal

* Corresponding author: Department of Civil Engineering, University of Minho, Campus de Azurém, Guimarães, 4800-058, Portugal; email: jpereira@civil.uminho.pt

Abstract: The vulnerability of the masonry envelop under blast loading is considered critical due to the risk of loss of lives. The behaviour of masonry infill walls subjected to dynamic out-of-plane loading was experimentally investigated in this work. Using confined underwater blast wave generators (WBWG), applying the extremely high rate conversion of the explosive detonation energy into the kinetic energy of a thick water confinement, allowed a surface area distribution avoiding also the generation of high velocity fragments and reducing atmospheric sound wave. In the present study, water plastic containers, having in its centre a detonator inside a cylindrical explosive charge, were used in unreinforced masonry infills panels with 1.7m by 3.5m. Besides the usage of pressure and displacement transducers, pictures with high-speed video cameras were recorded to enable processing of the deflections and identification of failure modes. Additional numerical studies were performed in both unreinforced and reinforced walls. Bed joint reinforcement and grid reinforcement were used to strengthen the infill walls, and the results are presented and compared, allowing to obtain pressure-impulse diagrams for design of masonry infill walls.

Keywords: Infill walls, Out-of-plane loading, Blast Loading, WBWG

1. Introduction

Only a few numerical or experimental studies have been conducted on impact and blast on structural components of building structures, characterized by strain rates well over 1 s^{-1}, with quasi-static tests characterized by strain rates in the range 10^{-5} to 10^{-7} s^{-1}. There is a need for more research to obtain an accurate representation of the effect of blasts, as high nonlinear behaviour and possible brittle failure has been observed. The out of plane vulnerability of the masonry envelop under dynamic loading is considered critical due to the risk of loss of lives, emphasized by many studies, particularly in the case of earthquakes [1], and explosion debris [2]. Nevertheless, earthquake resistant buildings are unlikely to meet the direct effects of a blast acting on the exterior skin of a building. Some reasons for the differences are: (a) explosions act directly on the exterior envelope whereas earthquakes are due to movements at the base; (b) explosions generally cause localized damage whereas earthquakes generally cause a global response. Still, only a few laboratory experimental investigations seem available in literature, simulating vehicles impacts on parapets [3] and air-blasting [4].

A key issue on the mechanical behaviour under blast is the strength increase due to high-strain rate. Explosions produce very high strain rates, usually around $10^2 – 10^4$ s^{-1}. Reinforced concrete structures, for example, are highly affected by this phenomenon. Its resistance can increase greatly, with dynamic increase factors as high as 4 in compression and 6 in tension reported [5][6]. In the case of masonry and its components the available studies are limited. Recently, dynamic increase factors higher than 2 in compression for clay brick were reported [7][8].

This paper presents a newly developed test setup for dynamic out-of-plane loading using underWater Blast Wave Generators (WBWG) as loading source. Underwater blasting operations have been, during the last decades, subject of research and

development of maritime blasting operations (including torpedo studies), aquarium tests for the measurement of blasting energy of industrial explosives and confined underwater blast wave generators. WBWG allow a wide range for the produced blast impulse and surface area distribution. It also avoids the generation of high velocity fragments and reduces atmospheric sound wave [9][10]. With the new setup, an unreinforced masonry infill wall subjected to blast loading is tested. Thereafter, three different masonry wall solutions are studied numerically, namely unreinforced masonry infill walls and two different reinforcement solutions. These solutions have been studied previously for seismic performance [11]. Finally, charts are created and presented to help designers to make informed decisions on the use of masonry infills under blast loading.

2. Test setup for dynamic out-of-plane loading

This work was performed in collaboration with LEDap (Laboratory of Energetics and Detonics) in Condeixa-a-Nova, Portugal. The developed test setup was constructed at LEDap facilities and comprises several elements. A support steel structure holds the specimen in place and provides sufficient reaction to the wall's reinforced concrete frame, Figure 1a. On one side of the wall a number of large (one cubic metre) water containers are placed to act as WBWG and apply the desired load. On the other side of the wall, measuring equipment is placed is order to characterize the behaviour of the wall. The maximum deflection is measured using laser equipment and high speed video cameras are used to record the wall during the test. All the area is surrounded by protection walls and a safe area was defined to provide safe hosting for the acquisition equipment and personal during the tests, Figure 1b.

2.1. Blast wave generator

The original blast wave generators (BWG), from the direct application of an explosion in air with high explosives, have the inconvenient of producing hot polluted gases, providing a reduced area of induced pressure, allowing the possibility of generation of high velocity fragments and producing a very intense sound wave. Using confined underwater blast wave generators (WBWG), applying the extremely high rate conversion of the explosive detonation energy into the kinetic energy of a thick water confinement, allows a surface area distribution. This also avoids the generation of high velocity fragments and reduced the atmospheric sound wave [12].

Since the physical properties of water and air are different, the characteristics of the shock waves (in air and water) are also different, mainly due to density and shock wave velocity (shock impedance) of the materials. The density of water is about 800 times greater than the density of air, while the sound velocity in water is 1500 m/s and the sound velocity in air is about 330 m/s (4.5 times faster). Therefore, the shock wave in water is 4.5 times faster than in air, and the pressure impulse for the shock wave in water is 15-20 times higher than in air [9]. After the detonation of an explosive charge under water, the detonation products expand generating shock wave in water and forming a gas bubble. This gas bubble expands and the pressure inside the bubble decreases. Because of inertia of water flow in front of the bubble, the expansion of the gas bubble continues even after the pressure inside the bubble decreases slightly below the pressure of the surrounding water. Afterwards, the pressure inside the gas bubble drops below the pressure of the surrounding water and the gas bubble movement stops [12]. However, the phenomenon does not fully stop as the gas bubble contracts under the action of surrounding pressure. The contractions and expansions continue for

several cycles, which generate pulsating movement in the gas bubble and additional compression waves in the water [9].

In the tests carried out in this work, the explosive charge was placed in the centre of the water container (Figure 2). The explosive used in the tests was PETN (pentaerythritol tetranitrate), a highly explosive organic compound. For the first level of loading, 7.2 g of PETN were used in each water container.

These common water containers have a metallic protection mesh surrounding them, which needed to be cut on the side facing the wall, in order to have full contact. The metallic mesh on the remaining sides was left in place to help keeping the water volume (Figure 3a). Due to the size of the wall under study (3.5×1.7 m) six water containers were used, being two rows of 3 water containers on top of each other. The procedure for placing the water containers was the following: a) prepare all metallic meshes as indicated; b) place the first row of containers in their final position; c) place the explosive charge in the centre of the container (using a thin tube to guide and to keep the charge in place); d) fill the first row of containers with 3000 litres of water (Figure 3b); e) place a wooden board on top of the first row to help distributing the weight of the second row; f) place the second row of containers (Figure 3c); repeat steps c) and d).

2.2. Pressure/deflection acquisition

One of the main issues regarding dynamic testing, which is blast loading in this case, is the proper acquisition of signals. The measuring equipment needs to have capacity for high acquisition frequencies. In this work there were two signals that needed to be recorded: a) the pressure profile acting on the wall; and b) the deflection profile of the wall.

For the pressure acquisition, a new sensor was developed. The mechanism used to measure the pressure consists of an assembled instrumental stainless steel plate between the wall and the water container. The pressure is measured using a tube connected to a sensor. This tube contains thin oil and is connected in a closed loop. The pressure device works like a force multiplier that provides hydrostatic pressure transmission. The pressure sensors used were 4-20 mA Gems^{TM} Sensors and Controls 3100B0016(10)G01B. In order to plot the acquired pressure signal, these sensors were connected to a Tektronix TDS 320 oscilloscope. This sensor was previously tested and calibrated [9][10].

For the deflection acquisition, a Keyence CMOS Multi-Function analogue laser sensor IL-2000 with a signal amplifier IL-1000 was used. This sensor was connected to a National Instruments acquisition system composed of a SCXI-1000DC chassis, a SCXI-1600 data acquisition and a control card for PC connection and a generic input module SCXI-1520 with a SCXI-1314 mount. In this case the sampling rate was limited by the laser sensor and was set at 3 kHz. With this system, it is possible to measure only the deflection of one point in the wall, which was the centre point of the wall, see Figure 4.

Besides the usage of pressure and displacement transducers, high speed video equipment was used to study the behaviour of the wall during the test. Three different cameras were used, marked in Figure 1b as camera A, B and C. Camera A is a PHOTRON APX-RS and was placed to have a full view of the wall. This camera was set with an acquisition frequency of 1 kHz. Cameras B and C are Casio EX-FH25 and were placed with different angles. Camera B was placed on the side of the wall in order to capture the profile of the wall. Camera C was placed in order to capture the WBWG and their behaviour during the test. Both cameras were set with an acquisition frequency

of 0.4 kHz. To help having a better view of the movement of the wall, a regular mesh was drawn in the wall using black tape, Figure 4.

2.3. Test specimen

The test setup detailed was developed for testing the dynamic out-of-plane behaviour of infill masonry walls. The adopted solution for the infill masonry represents the single leaf infill walls in modern construction, usually complemented by an external insulation. The masonry infill is built inside a reinforced concrete (RC) frame that provides the boundary conditions. The final dimensions of the test specimen can be seen in Figure 5a, which are made in a 1:1.5 scale. This is an unreinforced single leaf infill with 30×20×15 cm brick (labelled URM), with 15 mm cover on each side (Figure 5b). M5 plaster is used on one side and projected gypsum is used on the other side. Additional information on these specimens can be found on [11][13].

The construction process of the walls consists of the following steps: 1st) construction of the RC frames; 2nd) construction of the masonry infill panel; 3rd) execution of plaster. The placement of the masonry is done by successive horizontal rows, always from the columns. For the first masonry unit, mortar is applied on the bed and head faces. The unit is then pressed against lower beam and column. The last unit in each horizontal row is cut in order to ensure dimensional compatibility, as usually done in practice.

3. Test Execution and Results

The traditional construction process for building masonry infills was already described. In this specific work, additional steps had to be taken because the wall could not be built already in its final position. First, the reinforced concrete frame was built outside the testing site (Figure 6a). After curing, the frame was transported and placed in front of

the support structure (Figure 6b). At that location, the masonry infill was built with the process described before (Figure 6c). After curing the wall, the plaster and the projected gypsum were applied to the wall (Figure 6d). After building the masonry wall, it had to be slightly moved towards the support structure using heavy machinery (Figure 6e). With the wall in its final position, the reinforced concrete frame was bolted to the steel support structure in eleven marked places along its perimeter (Figure 6f).

With the wall specimen ready to be tested, the loading containers and data acquisition equipment needed to be put in place. As shown before, the water container were placed and filled in two phases. Meanwhile all the sensors and acquisition systems are mounted and tested (Figure 7a). The final step before the test itself is connecting the detonators (Figure 7b). Due to the dangerous nature of these tests, all systems need to be triple checked before this final step. After placing the detonators, nobody is allowed into the test site and every system is controlled from the designated safe area. The acquisition systems start and a countdown is set until detonation.

After the test, the acquired signals need to be processed. The oscilloscopes provided the applied pressure on the wall and the final pressure profile was plotted, Figure 8. As can be seen in Figure 8, two pressure sensors were used, however one of the sensors failed to acquire after a few milliseconds of testing. It is possible to see that the initial parts of the sensors are quite similar, although only one sensor captured the full length of the test and was used to define the applied pressure on the wall surface. The pressure rises up to 149 kPa in the first 6 ms, then decays and reaches 119 kPa at 17.5 ms and stops acting after 29 ms. From the laser sensor, the deflection on the central point of the wall was obtained, Figure 9. The deflection on the wall has an expected profile, increasing until its maximum of 14.6 mm after 24 ms and has a residual value of around 11 mm.

Besides these profiles, the video acquired with the high speed cameras was also analysed. Figure 10 shows pictures taken from those videos at specific times. Due to the magnitude of the deformations (small when compared with the dimensions of the wall) it is difficult to perceive the evolution of deformations in just a few static pictures. However, analysing the slow motion video, it is possible to see the full behaviour of the wall. The maximum displacement is achieved at the centre point of the wall, which behaves as a plate supported in its four edges.

After the test, a visual inspection of the wall was also performed. The cracks were marked in order to have a view of the crack pattern (Figure 11a). There is a large concentration of large horizontal cracks at the centre of the wall (Figure 11b) and these spread to the corners, as they move away from the centre. There are also some large cracks at the top support edge.

4. Numerical modelling

The global field of structural analysis of masonry structures encompasses several different approaches and a review is given by [14]. In general, the approach towards the numerical representation of masonry can address the micro modelling of the individual components: unit (brick, block, etc.) and mortar; or the macro modelling of masonry as a composite. Depending on the level of accuracy and the simplicity desired, it is possible to use the following modelling strategies: a) detailed micro-modelling, where units and mortar in the joints are represented by continuum elements whereas the unit-mortar interface is represented by discontinuum elements; b) simplified micro-modelling, where expanded units are represented by continuum elements whereas the behaviour of the mortar joints and unit-mortar interface is lumped in discontinuum elements; c) Macro-modelling, where units, mortar and unit-mortar interface are

smeared out in a homogeneous continuum. Many approaches involving different approximations and ingenious assumptions have been sought, e.g. [15][16][17], where simplified non-linear homogenization techniques were used.

This numerical analysis was performed using a Finite Element Model (FEM). The geometry model was based on the description provided in section 2.3. Only the infill panel was modelled and a perfect connection was considered between the infill panel and the reinforced concrete frame (Figure 12a). A macro-modelling strategy was adopted, where the panel is considered a homogeneous continuum. The FEM model was built in the ABAQUS software [18], where the Explicit solver was used. This software has been used successfully in previous situation regarding similar loading conditions [19][20][21] and similar materials [22][23]. The wall was discretized with 8-node solid elements (C3D8R) with reduced integration and hourglass control (ABAQUS User Manual, 2010). The final mesh was automatically generated by ABAQUS, and is rather refined. The edges were considered constrained in all degrees of freedom. The thickness of the wall was set as 180 mm (brick plus plaster on both sides). The final mesh has 4872 elements and 6844 nodes (Figure 12b).

4.1. Material model

The CDP (Concrete Damaged Plasticity) model used in ABAQUS software is a modification of the Drucker-Prager model by [24][25]. In particular, the shape of the failure surface in the deviatoric plane needs not to be a circle and it is governed by parameter K_c. This parameter can be interpreted as a ratio of the distances between the hydrostatic axis and, respectively, the compression meridian and the tension meridian in the deviatoric plane. This ratio is always higher than 0.5 and when it assumes the value 1, the deviatoric cross section of the failure surface becomes a circle [26]. The CDP

model requires four additional parameters to be defined: a) the dilatation angle; b) the flow potential eccentricity: c) the ratio of initial equibiaxial compressive yield stress to initial uniaxial compressive yield stress; and d) the viscosity parameter. For all these five parameters the default values suggested in ABAQUS User's Manual were used (Table 1). Additional information regarding this model can be found in [18][26][27].

The CDP model assumes that the failure for tensile cracking and compressive crushing of the material is characterized by damage plasticity. The model uses the concept of isotropic damage evolution in combination with isotropic tensile and compressive plasticity to represent the inelastic and fracture behaviour of the material. The model also allows the definition of strain hardening in compression and strain softening in tension. The adopted stress-strain curves have exponential softening in tension and parabolic hardening followed by exponential softening in compression.As stated previously, a similar masonry wall was tested and mechanically characterized under quasi-static conditions. The data collected from [11] regarding the quasi-static mechanical properties for the single leaf infill wall with plaster on both sides can be seen in Table 2. The quasi-static properties obtained from the quasi-static tests serve as a base for the calibration of the numerical model. The mechanical properties under dynamic conditions will be subsequently obtained by matching the deflection of the numerical model with the experimental data.

4.2. Explicit analysis

ABAQUS Explicit was used to solve the non-linear equations of this problem. In order to keep this problem within a pure Lagrangian formulation, the blast loading was defined as a pressure profile. The blast loading applied was derived from the obtained experimental data (Figure 8). As stated previously, a key issue on the mechanical

behaviour under blast is the strength increase due to high-strain rate. The strain rate influence on the material properties are introduced as DIF, which are variable with the strain rate [8][9]. However, the available strain rate dependant constitutive models were not developed for masonry. For this analysis, the DIF increase due to strain rate effects was simplified and considered constant. The calibration process started with the application of the static reference mechanical properties. After realizing that the displacement obtained was much higher than the obtained experimentally, the mechanical properties were increased until there was a good agreement between the numerical model and the experimental data. The final dynamic properties and the respective dynamic increase factor (DIF), considering constant DIF, can be seen in Table 3. This process is not fully objective but, the obtained results are in agreement with the conclusions obtained in other research for the masonry specimens, where DIF between 2 and 3 for the compressive strength and the Young's modulus [7][8].

Figure 13 shows the result from the numerical model in terms of displacement vs. time and compares it with the experimental data. There is a good initial agreement up to 12 mm in deformation. At this instant the experimental curve changes its slope, probably due to appearing cracks. The maximum displacement has a difference of 3%. In the post-peak behaviour there is some difference between the experimental and the numerical model, but it can still be considered acceptable. In the experimental test the wall was able to set its residual deformation at 76% of the maximum deformation. In the numerical model the residual deformation was 91%. In the experimental test, when the blast wave from the WBWG reaches the wall it generates an expansion wave that travels through the thickness of the wall. When this expansion wave reaches the opposite edge of the wall it will start moving in the opposite direction creating a "negative" wave profile, which was not considered in the numerical model. This can

justify part of the difference. It is also possible that there is some sliding in the test, particularly, in the top crack, which is not considered in the model.

Besides the comparison of the deflection profile, the damage on the wall was also compared. The maximum principal plastic strains are a reasonable indicator of cracking and were plotted in Figure 14 for the face on the back of the explosion. As expected, according to this model, there is a concentration of cracks at mid height of the wall that will start to spread to the corners as we move further from the centre point. There is also some damage at the bottom and top edge of the wall. These results are in agreement with the observed damage in the experimental test (Figure 11).

4.3. Reinforced solutions

Numerical models for reinforced solutions were prepared considering the following possibilities, as done by [11]: a) single leaf infill with 30×20×15 cm brick with bed joint reinforcement (labelled JAR); b) single leaf infill with 30×20×15 cm brick with external reinforcement in the plaster and plaster in both sides (labelled RAR).

Both solutions adopt only slight amounts of reinforcement, as typically used for crack control. The first reinforcement solution under study – JAR – has bed joint reinforcement type BEKAERT MURFOR RND .4/100 every two horizontal joints. The adopted geometry for the numerical model can be seen in Figure 15 and comprises the previous model with the addition of 8 reinforcement bars embedded in the masonry region. Each reinforcement bar has a cross section area of 12.57 mm^2. The second solution for reinforcement under study – RAR – has a mesh type BEKAERT – ARMANET Ø1.05 mm 12.7×12.7 mm in both sides of the wall, embedded in the plaster. An equivalent reinforcement grid with 87.55×87.55 mm openings was added to

the unreinforced model (Figure 16). Each reinforcement bar has a cross section area of 5.97 mm^2.

The reinforcement elements, for both models, were truss elements T3D2 which is a 2 node linear 3D truss for explicit analysis [18]. For the material properties an elastic-ideal plastic model was adopted. The static mechanical properties for the reinforcement were collected from the product datasheets. Because there was no experimental work performed on the material properties at high strain rates for these reinforcement bars, the recommended DIF in [28] was used. This standard indicates a DIF of 1.23 for the tensile strength of reinforcement steel in bending. The dynamic properties for this material can be seen in Table 4.

Figure 17 shows the result obtained for the displacement at the centre point of the wall considering both reinforcement solutions and compares it with the unreinforced model. As can be seen, both solutions show an improvement in the response of the structure. The solution considering bed joint reinforcement decreases the maximum displacement of the wall in 25% and the solution with the grid reinforcement decreases the maximum displacement in 50%. These solutions have been studied for seismic action mitigation and the results reported for that specific application suggest that both reinforcement solutions improve the response of the out-of-plane behaviour of masonry walls [13]. However, the obtained response seems to be similar for both reinforcement solutions under cyclic combined in-plane and out-of-plane loading using airbags [13]. The results are hardly comparable as there is no in-plane action in the present case. The numerical analysis for impulsive loading carried out suggests a considerable difference between both reinforcement solutions.

Certainly, higher improvements in the response of the wall could be obtained by increasing the amount of reinforcement added. Figure 18 shows the maximum displacement for the URM wall and compares it with three different solutions for the bed joint reinforcement: JAR 4mm – bed joint reinforcement with .4/100 in every two horizontal joint; JAR 5mm – bed joint reinforcement with .5/100 in every two horizontal joint; and JAR all joints – bed joint reinforcement with .4/100 in every horizontal joint. As can be seen in Figure 18 the improvement with increasing the amount of reinforcement is not proportional to the reinforcement ratio. Thus, it is reasonable to assume that the behaviour is rather dependant on the compressive behaviour of masonry. This can be seen in Figure 19, where another analysis was performed with the minimum JAR reinforcement and a masonry with double compressive strength (f_c = 7.5 MPa). Doubling the compressive strength of masonry, the response (in terms of maximum displacement) is less than half.

In order to have a better grasp on the influence of these minimum reinforcement solutions, additional model were studied for different wall thickness. A thickness of 140 mm and 230 mm were studied, the selected values for the thickness of the wall were determined assuming the use of 30×20×11 cm^3 and 30×20×20 cm^3 bricks plus same plaster on both sides, even if plaster is usually not considered for design purposes. Figure 20 shows the obtained results for the minimum reinforcement solutions for these two different thickness walls. The grid reinforcement was the same for both models, but the bed joint reinforcement needs to use commercially available products. RND .4/80 and RND .4/150 trusses were used for the 140 mm and the 230 mm respectively. It can be seen that the grid reinforcement has a higher improvement in the response of the wall for both models. These results show that the response of the wall to these impulse loadings is highly influenced by its thickness, as expected. The same loading profile

resulted in maximum deformations of about 400 mm, 15 mm and 3 mm for increasing thickness of 140 mm, 180 mm and 230 mm respectively.

4.4. Parametric study

In order to discuss the influence of the mechanical and geometric properties of masonry infill panels on the blast response, a parametric study was performed. For this kind of analysis it is important to understand this influence as a function of the impulsive loading. This can be obtained by varying the applied load according to the scaled distance Z ($Z = R/W^{1/3}$ [m/kg$^{1/3}$]), which depends on the weight of the explosive (W) and the standoff distance (R). Knowing the weight of the explosive and its standoff distance it is possible to determine the applied reflected pressure for different loading scenarios using Eqs. (1) – (3) developed for point source explosions [29][30][31].

$$P_{S0} = 6784\frac{W}{R^3} + 93\left(\frac{W}{R^3}\right)^{\frac{1}{2}} \tag{1}$$

$$P_r = 2P_{S0}\left(\frac{7P_0 + 4P_{S0}}{7P_0 + P_{S0}}\right) \tag{2}$$

$$t_D = 10.23\frac{W^{1/3}}{\sqrt{P_{SO}}} \tag{3}$$

Here P_{S0} is the side-on overpressure, P_r is the reflected pressure and t_d is the positive duration.

Table 5 shows the range of properties selected for this parametric study. The tensile and the compressive strength range from the static reference value up to a DIF equal to 5. The Young's modulus ranges from its static reference up to a DIF equal to 3 and the fracture energy ranges from its static reference up until a DIF equal to 4. The selected values for the thickness of the wall were determined assuming the use of 30×20×11 cm^3

and 30×20×20 cm^3 bricks plus same plaster on both sides. The reinforcement can either be absent (URM), in the bed joint (JAR) or in the plaster (RAR). Unless stated otherwise, when varying a selected property the remaining properties are kept at their mid values.

The compressive strength, Figure 21a, has a considerable influence on the maximum displacement of the wall, for smaller scaled distances. This influence appears to fade once a certain level of compressive strength is achieved, which means that from a certain point there is no real advantage in increasing the compressive strength. The Young's modulus, Figure 21b, influences the maximum displacement of the wall at all levels of scaled distance. When analysing the tensile strength, Figure 21c, it is possible to see the same behaviour of that the compressive strength, with a similar conclusion. When varying the tensile strength, the fracture energy was also changed in the same proportion as the tensile strength. The Mode I-fracture energy, Figure 21d, only influences the maximum displacement at smaller scaled distances. Here, the tensile strength was kept the same for all models. The thickness of the wall, Figure 21e, is one of the parameters with larger influence on the maximum displacement of the wall. As seen before, the use of reinforcement solutions decreases the maximum displacement of the wall, but only to moderate extent for the (low) amounts of reinforcement used. Figure 21f shows that this influence is inversely proportional to the scaled distance.

4.5. Pressure-Impulse diagrams

Pressure-Impulse diagrams are empirical tools that allow a given load-impulse combination, which will cause a specific level of damage, to be assessed readily [29]. These diagrams can be used to assess a specific loading profile which caused certain damage to an element, in a post-disaster scenario. On the other hand, these tools can be

used at an early design stage to get an approximation of the damage to an element given a specific loading profile.

In order to make it easier for the designer to use these tools, for the structural elements under study, it is better to have damage criteria (Table 6) instead of pure deflection curves. For the present work, the criteria defined by [28] will be applied, meaning that instead of iso-deflection curves, the P-I diagrams were plotted with two levels of damage, reusable and non-reusable. With the FE model calibrated (Table 3), several simulations were performed for different levels of overpressures and impulses. For these numerical models a 1:1 scale was used, meaning that the masonry infill panels have an area of 5250 by 2550 mm^2. Two different masonry infill panels were studied, with 180 mm thickness and 230 mm thickness.

Figure 22 to Figure 24 present the obtained pressure-impulse diagrams for the three constructive solutions under study. As expected, the reinforced solutions are able to accommodate somewhat larger loading profiles and have the non-reusable and the reusable curves further away. This becomes clear when analysing Figure 25 for the 180 mm thickness and Figure 26 for the 230 mm thickness, where a comparison for the three constructive solutions under study is performed for both levels of damage. Of course, higher percentages of reinforcement can be used to obtain a specified performance but, here, the focus is given to the minimum amounts of reinforcement.

Figure 25 and Figure 26 show that if the damage level required is the reusable stage, there is no real advantage in using the minimum reinforcement solutions, for weak masonry infills and large panels. Only at the non-reusable stage the minimum reinforcement solutions have a relevant contribution for the wall's response.

These P-I diagrams can be used to select the proper constructive solution regarding a specific level of blast loading under design. As can be seen from Figure 22 to Figure 26, the thickness of the wall is one important aspect to account for. The grid reinforcement is the solution with the highest mechanical improvement regarding the maximum displacement of the wall. Another important aspect regarding this reinforcement solution is that it also protects against the appearance of flying debris into, possibly, occupied areas.

5. Conclusions

A newly developed test setup for dynamic out-of-plane testing on walls was presented, including the developed sensors and acquisition apparatus. Using underwater blast wave generators (WBWG) it was possible to have a surface area distribution of pressure avoiding the generation of high velocity fragments and reducing atmospheric sound wave. Also the required test site area can be greatly reduced using these WBWG as opposes to traditional air blast, where to have a full surface distribution the charge need to be far away from its target.

One unreinforced masonry infill panel was tested under blast loading using underwater blast wave generators and the results were presented. The obtained results were used to calibrate a numerical model using ABAQUS Explicit dynamics software. A good agreement between the numerical model and the experimental data was obtained, allowing a detailed study on this kind of masonry panels under dynamic out-of-plane loading in the form of a parametric study for different loading conditions and different properties of masonry. This parametric study showed that there is a point where the increase of the compressive and tensile strength is no longer effective (as the response becomes elastic), while the Young's modulus and the wall thickness are the parameters

with the higher influence on the behaviour of the wall panel. Two different reinforcement solutions were analysed numerically and the results show that both solutions improve the response of the wall, to a moderate extent, as the amounts of reinforcement are close to the minimum values (only for crack control). The reinforcement solution with the best performance under blast loading was the grid reinforcement in the plaster of the wall, as the amount of reinforcement is slightly higher.

These results were used to create empirical tools – Pressure-Impulse diagrams – which can help the designer to estimate the response of the element under different loading conditions. It was shown that the use of these (low percentage) reinforcement solutions is more effective considering the non-reusable stage of the element. If the requirement is the reusable stage there is no real advantage in the use of these (low percentage) reinforcement solutions, and the best way to improve the response of the wall would be increasing its thickness or designing the reinforcement according to the performance sought. More experimental data is required to confirm these findings and additional masonry infill walls should be tested.

6. Acknowledgement

This work was performed under Project CH-SECURE, with reference PTDC/ECM/120118/2010, funded by the Portuguese Foundation of Science and Technology – FCT. The authors acknowledge the support. The first author also acknowledges the support from his PhD FCT grant with the reference SFRH/BD/45436/2008.

7. References

[1] Calvi, G.M., Bolognini, D., Seismic response of reinforced concrete frames infilled with weakly reinforced masonry panels. Journal of Earthquake Engineering, 5(2), pp. 153-185, 2001.

[2] Wu, C., Hao, H., Safe scaled distance for masonry infilled RC frame structures subjected to airblast loads. Journal of Performance of Constructed Facilities, 21(6), pp. 422-431, 2007.

[3] Gilbert. M., Hobbs, B., Molyneaux, T.C.K., The performance of unreinforced masonry walls subjected to low-velocity impacts: experiments. International Journal of Impact Engineering, 27(3), pp. 231-251, 2002.

[4] Mayrhofer, C., Reinforced masonry walls under blast loading. International Journal of Mechanical Sciences, 44(6), pp. 1067-1080, 2002.

[5] Grote, D., Park, S., Zhou, M., Dynamic behaviour of concrete at high strain rates and pressures. Journal of Impact Engineering, 25(9), pp. 869-886, 2001.

[6] Ngo, T., Mendis, P., Hongwei, M., Mak, S., High strain rate behaviour of concrete cylinders subjected to uniaxial compressive impact loading. In Proc. of the 18th Australasian Conference on the Mechanics of Structures and Materials, Australia, 2004.

[7] Hao, H., Tarasov, B.G., Experimental study of dynamic material properties of clay brick and mortar at different strain rates. Australian Journal of Structural Engineering, 8(2), pp. 117-132, 2008.

[8] Pereira, J.M., Dias, A., Lourenço, P.B.: Dynamic properties of clay brick at different strain rates. In: Proc. of the 12th Canadian Masonry Symposium. Canada 2013.

[9] Tavares, B., Mendes, R., Plaksin, I. Campos, J., Santos, P.M.S., Duarte, B.P.M., Oliveira, N.M.C., Pereira, J.M., Lourenço, P.B., Prediction and experimental results of confined underwater blasting generators. In Proc. of the 2nd Korean International Symposium on High Energy Materials – KISHEM. Korea 2012.

[10] Ambrósio, J., Ferreira, R., Mendes, R., Campos, J., Pereira, J.M., Lourenço, P.B., Prediction and experimental results of confined underwater blasting generators. In Proc. of the 44th International Conference of the Fraunhofer ICT, Germany 2013.

[11] Pereira, M.F.P., Assessment of the building envelope subjected to seismic action (in Portuguese). PhD Thesis, Department of Civil Engineering of University of Minho, Portugal 2013.

[12] Plaksin, I., and Campos, J., Blast wave generator based on PBX enclosed in water container. In Proc. of the 5th European Symposium on Non-Lethal Weapons, Germany 2007.

[13] Pereira, M.F.P., Pereira, M.F.N., Ferreira, J.E.D., Lourenço, P.B., Behaviour of damaged masonry infill panels in RC frames subjected to out of plane loads, In Proc. of the 7th International Conference on Analytical Models and New Concepts in Concrete and Masonry Structures, Poland 2011.

[14] Lourenço, P.B., Mendes, N., Ramos, L.F., Oliveira, D.V., Analysis of masonry structures without box behavior, International Journal of Architectural Heritage, 5, p. 369-382, 2011..

[15] Gambarotta, L., Lagomarsino, S., Damage models for the seismic response of brick masonry shear walls. Part II: the continuum model and its applications. Earthquake Engineering & Structural Dynamics, 26(4), pp. 441-462, 1997.

[16] Massart, T.J., Peerlings, R.H.J., Geers, M.G.D., Mesoscopic modeling of failure and damage-induced anisotropy in brick masonry. European Journal of Mechanics-A/Solids, 23(5), pp. 719-735, 2004.

[17] Calderini, C., Lagomarsino, S., A micromechanical inelastic model for historical masonry. Journal of Earthquake Engineering, 10(4), pp. 453-479, 2006.

[18] ABAQUS User Manual, Dassault Systems Simulia Corporation, USA 2010.

[19] Cabello, B., Dynamic stress analysis of the effect of air blast wave on stainless steel plates. Msc Thesis, Faculty of Rensselaer Polytechnic Institute, USA 2011.

[20] Jacinto, A.C., Ambrosini, R.D., Danesi, R.F., Experimental and computational analysis of plates under air blast loading. International Journal of Impact Engineering, 25(10), pp. 927-947, 2001.

[21] Heidarpour, A., Bradford, M.A., Liu, J., Steel arches subjected to blast loading: a non-discretization analysis approach. Applied Mathematical Modelling, 36(9), pp. 3971-3984, 2012.

[22] Zheng, Y., Taylor, S., Robinson, D., Nonlinear finite element analysis of masonry arch bridges reinforced with FRP. In Proc. of the 6th International Conference on Arch Bridges – ARCH'10, China 2010.

[23] Al-Gohi, B.H., Demir, C., Ilki, A., Baluch, M.H., Rahman, M.K., Al-Gadhib, A.H., Seismic vulnerability of multi-leaf heritage masonry walls using elasto-plastic damage model. In Proc. of the International Workshop: Role of research infrastructure in seismic rehabilitation, Turkey 2012.

[24] Lubliner, J., Oliver, J., Oller, S., Onate, E., A plastic-damage model for concrete. International Journal of Solids and Structures, 25(3), pp. 299-329, 1989.

[25] Lee, J., Fenves, G.L., Plastic-damage model for cyclic loading of concrete structures. Journal of Engineering Mechanics, 124 (8), pp. 892-900, 1998.

[26] Kmiecik, P., Kaminski, M., Modelling of reinforced concrete structures and composite structures with concrete strength degradation taken into consideration. Archives of Civil and Mechanical Engineering, 11(3), pp. 623-636, 2011.

[27] Jankowiak, T., Lodygowski, T., Identification of parameters of concrete damage plasticity constitutive model. Foundations of Civil and Environmental Engineering, 6(1), pp 53-69, 2005.

[28] UFC 3-340-02, Structures to resist the effects of accidental explosions. Department of Defence, USA 2008.

[29] Cormie, D., Mays, G.C., Smith, P.D., Blast effects on buildings, 2nd edition. Thomas Telford Publications, England 2009.

[30] Bangash, M.Y.H., Bangash, T., Explosions – resistant buildings: design, analysis, and case studies. Springer Publications, Germany 2006.

[31] Ngo, T., Mendis, P., Gupta, A., Ramsay, J., Blast loading and blast effects on structures – an overview. Electronic Journal of Structural Engineering – special issue, 8, pp 76-91, 2007.

Tables:

Table 1: Default parameters of the CDP model.

Parameter	Value
Dilatation angle (Ψ)	20º
Eccentricity (ε)	0.1
f_{b0}/f_{c0}	1.16
K_c	0.667
Viscosity parameter (μ)	0.0

Table 2: Quasi-static mechanical properties [11].

Parameter	Static
Tensile strength, f_t [MPa]	0.125
Compressive strength , f_c [MPa]	1.24
Elastic modulus, E_0 [GPa]	3.6
Mode I-fracture energy, G_f^I [N/mm]	0.012

Table 3: Dynamic mechanical properties.

Parameter	Static	Dynamic	DIF
Tensile strength, f_t [MPa]	0.125	0.375	3
Compressive strength , f_c [MPa]	1.24	3.78	3
Elastic modulus, E_0 [GPa]	3.6	7.2	2
Mode I-fracture energy, G_f^I [N/mm]	0.012	0.025	2

Table 4: Dynamic mechanical properties for reinforcement.

Parameter	Static	Dynamic	DIF
Yield strength, f_y [MPa]	320	394	1.23
Elastic modulusE_0 [GPa]	210	210	1

Table 5: Properties range in the parametric study.

Parameter	**Min**	**Mid**	**Max**
f_t *[MPa]*	0.125	0.375	0.650
f_c *[MPa]*	1.26	3.78	6.30
E_0 *[GPa]*	3.6	7.2	10.8
G_f^I *[N/mm]*	0.012	0.025	0.050
Thickness [mm]	140	180	230
Reinforcement	JAR	URM	RAR

Table 6: Masonry damage criteria [28].

Element	Yield pattern	Maximum support rotation
Masonry Reusable	One-way	0.5º
	Two-way	0.5º
Masonry Non-reusable	One-way	1.0º
	Two-way	2.0º

Figures:

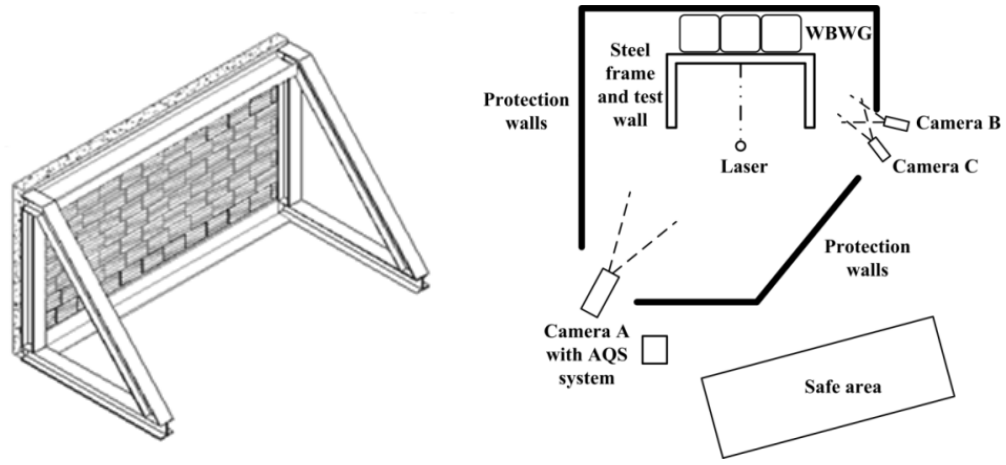

a) b)

Figure 1: Test setup: a) test specimen support; b) layout of the testing area.

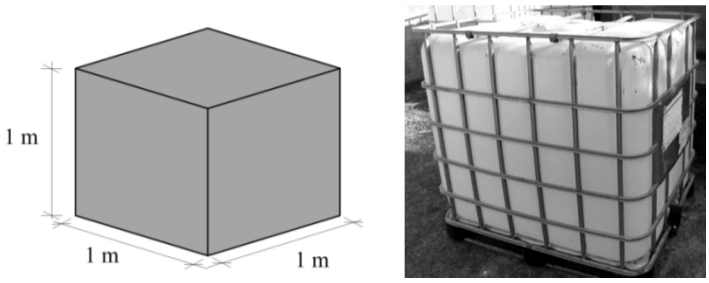

a) b)

Figure 2: Water container: a) schematic view; b) photo.

a) b) c)

Figure 3: Preparing the WBWG: a) cutting the metallic mesh; b) filling the first level of containers; c) both levels of containers in place.

a) b)

Figure 4: Laser sensor: a) final position; b) support system.

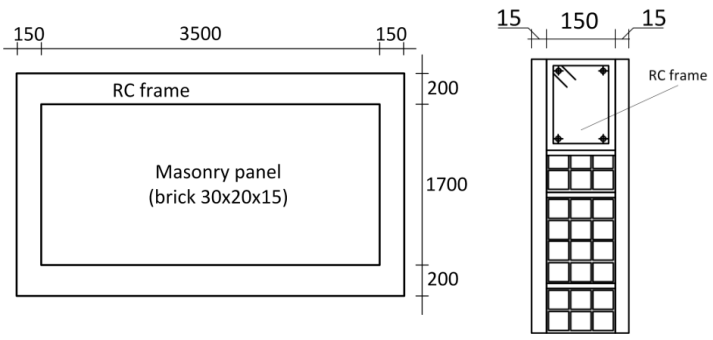

a) b)

Figure 5: Masonry specimens: a) geometry; b) schematics [dimensions in mm].

a)

b)

c)

d)

e)

f)

Figure 6: Building process and aspect of the specimen in the test setup.

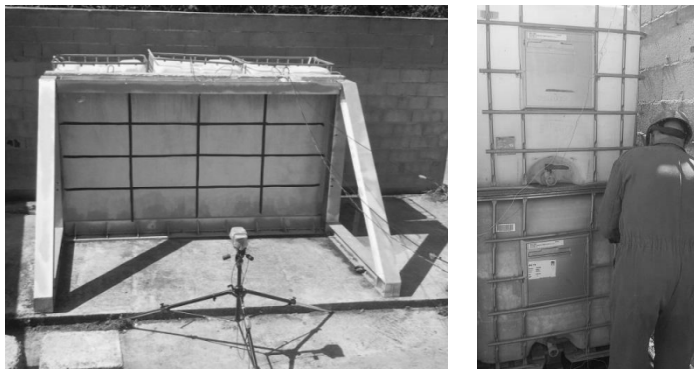

a) b)

Figure 7: Unreinforced wall test: a) all systems mounted; b) connecting the detonators.

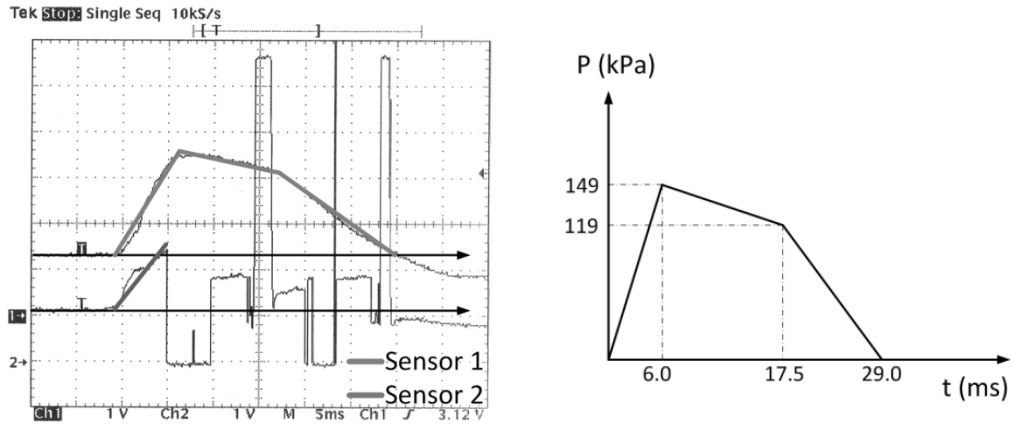

a) b)

Figure 8: Acquired pressure: a) from the oscilloscope; b) final pressure profile.

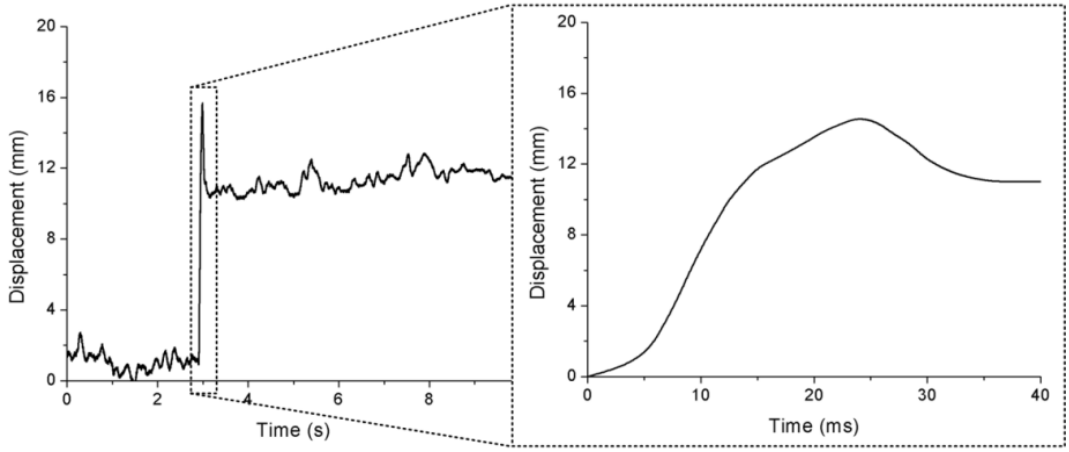

Figure 9: Displacement at midpoint acquired with laser.

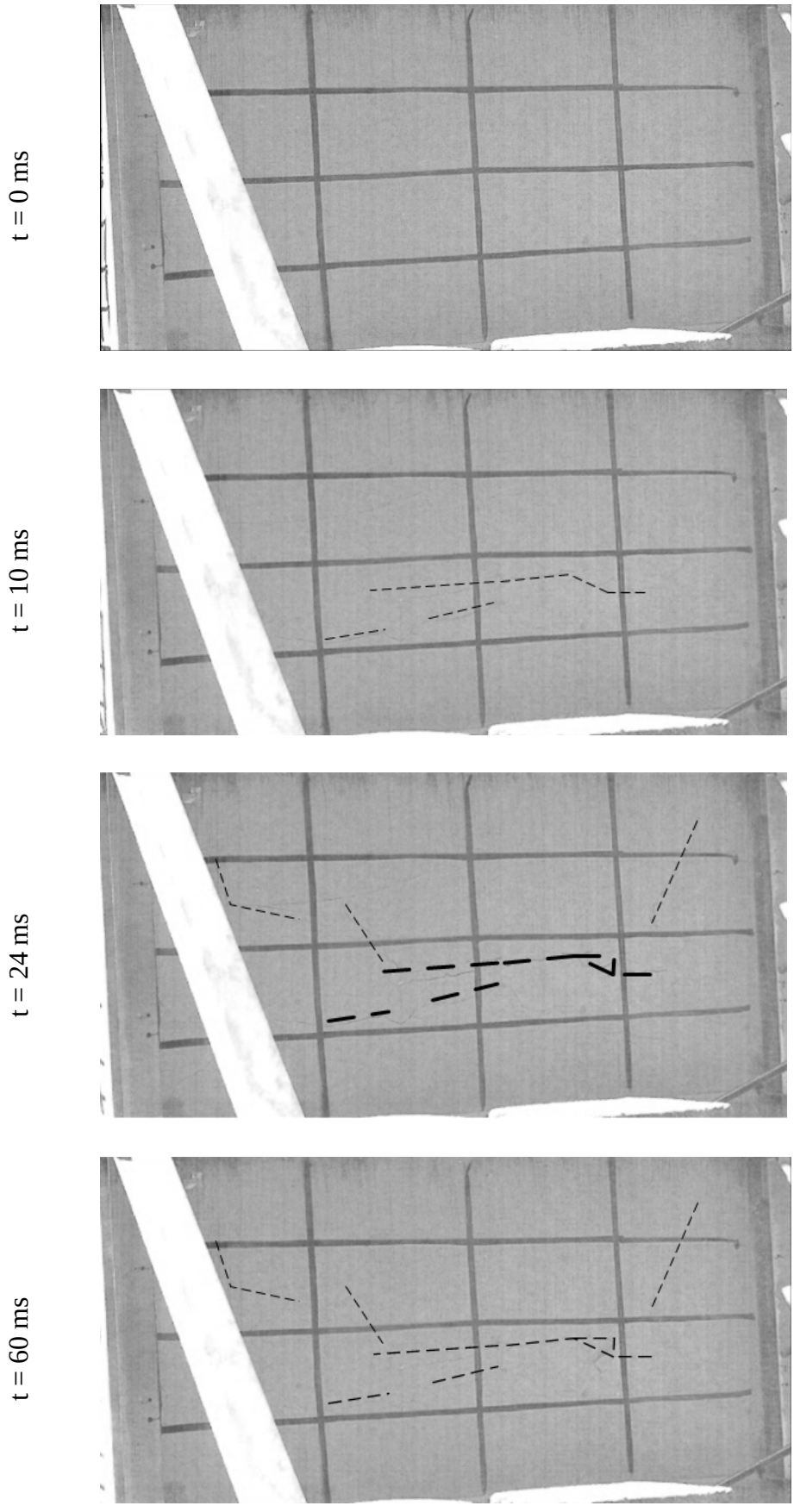

Figure 10: Pictures from video at Camera A at different instances.

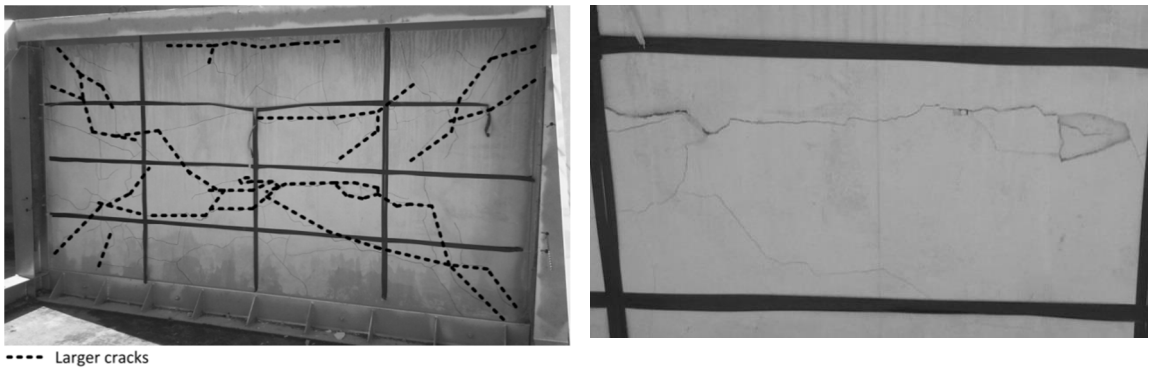

a) b)

Figure 11: Damaged wall after blast test: a) full panel; b) zoom on the centre of the panel (2nd row and 3rd column quadrant, from bottom-left corner).

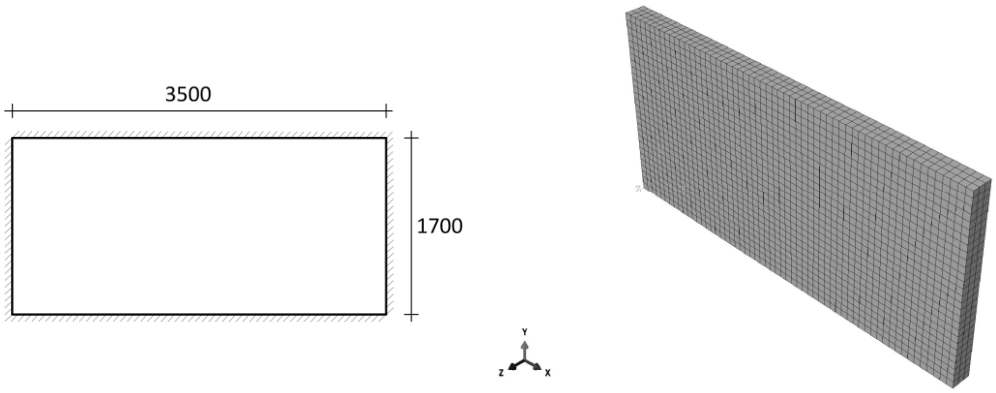

a) b)

Figure 12: FEM model: a) geometry; b) FE mesh.

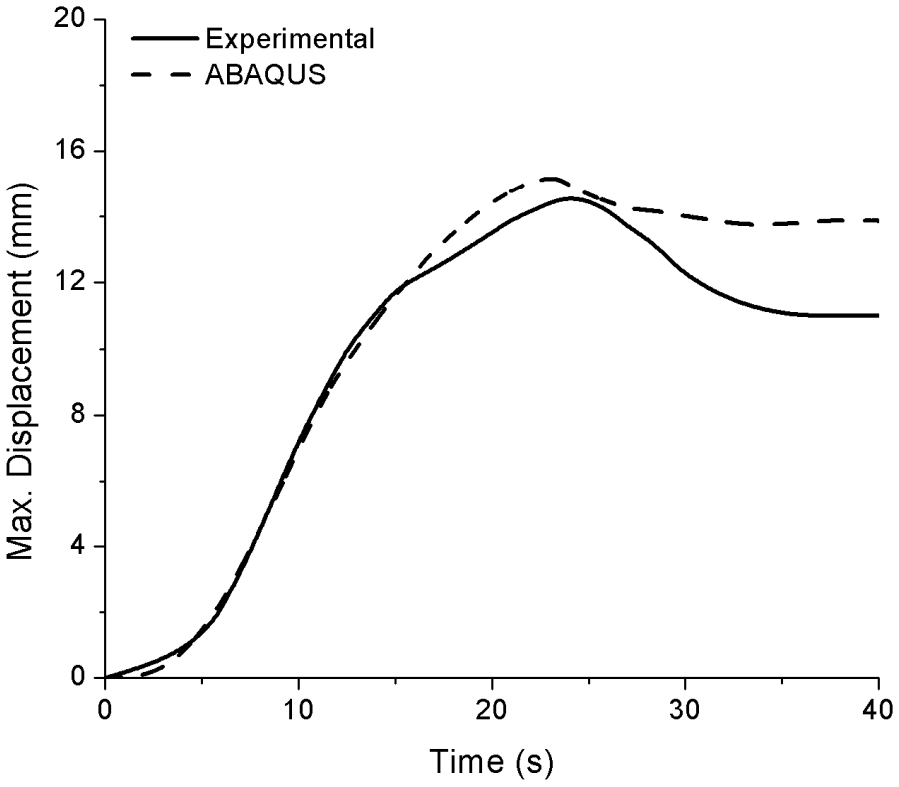

Figure 13: Comparison between the numerical model and the experimental data.

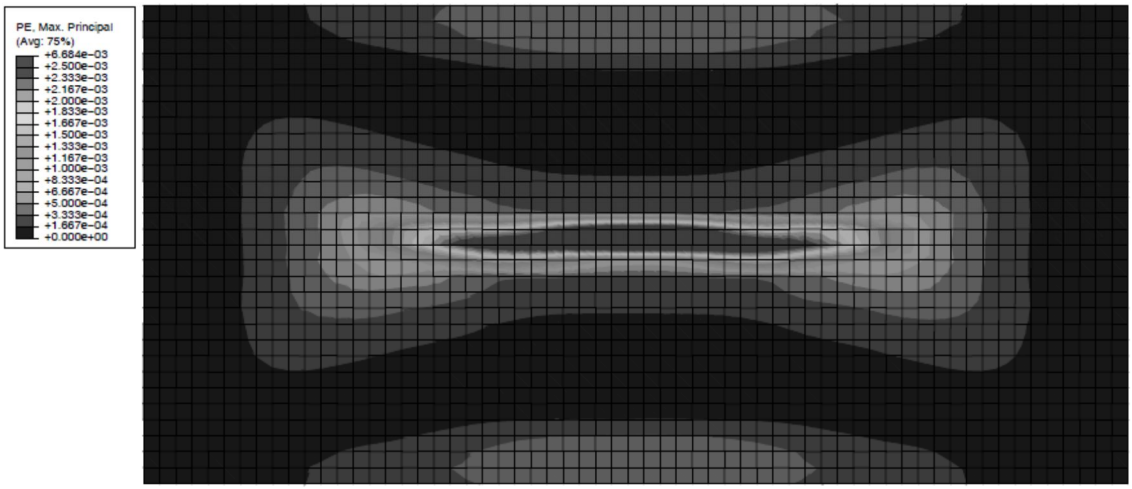

Figure 14: Maximum principal plastic strain in the external face of the wall.

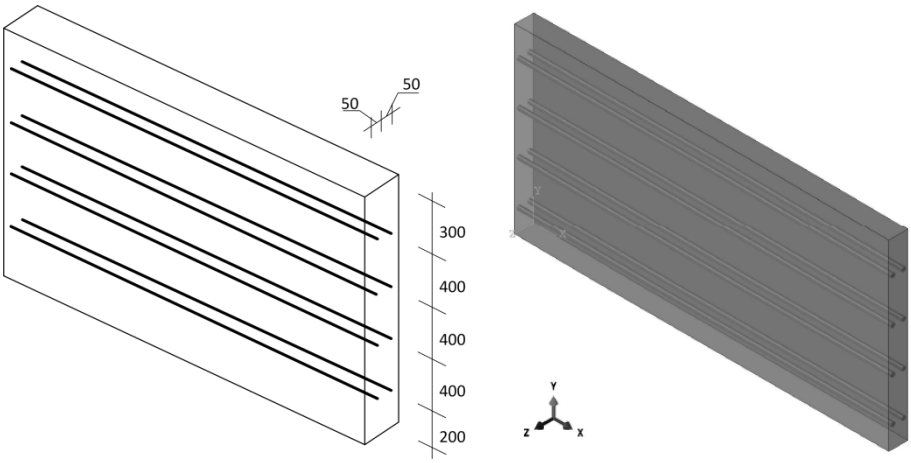

a) b)

Figure 15: JAR solution: a) geometry; b) assembly view from the numerical model.

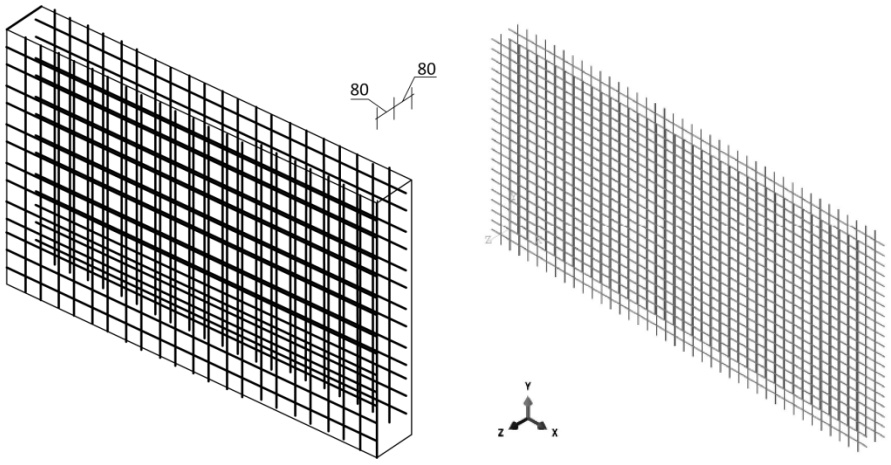

a) b)

Figure 16: RAR solution: a) geometry; b) reinforcement grid.

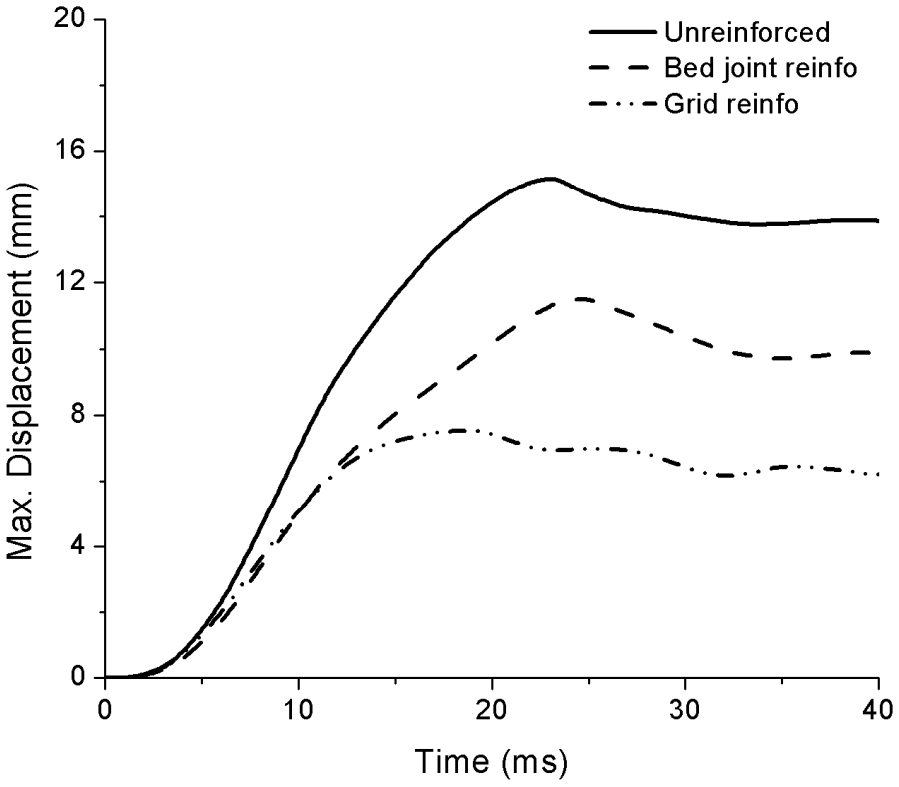

Figure 17: Influence of reinforcement in the response of the wall.

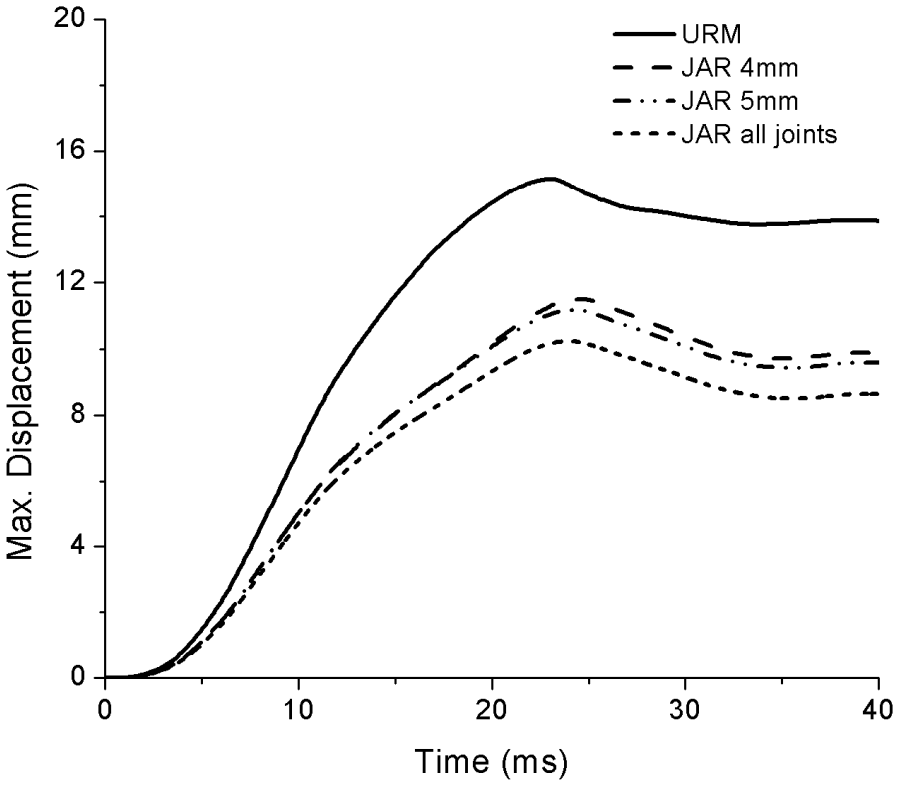

Figure 18: Influence of the amount of reinforcement in the response of the wall.

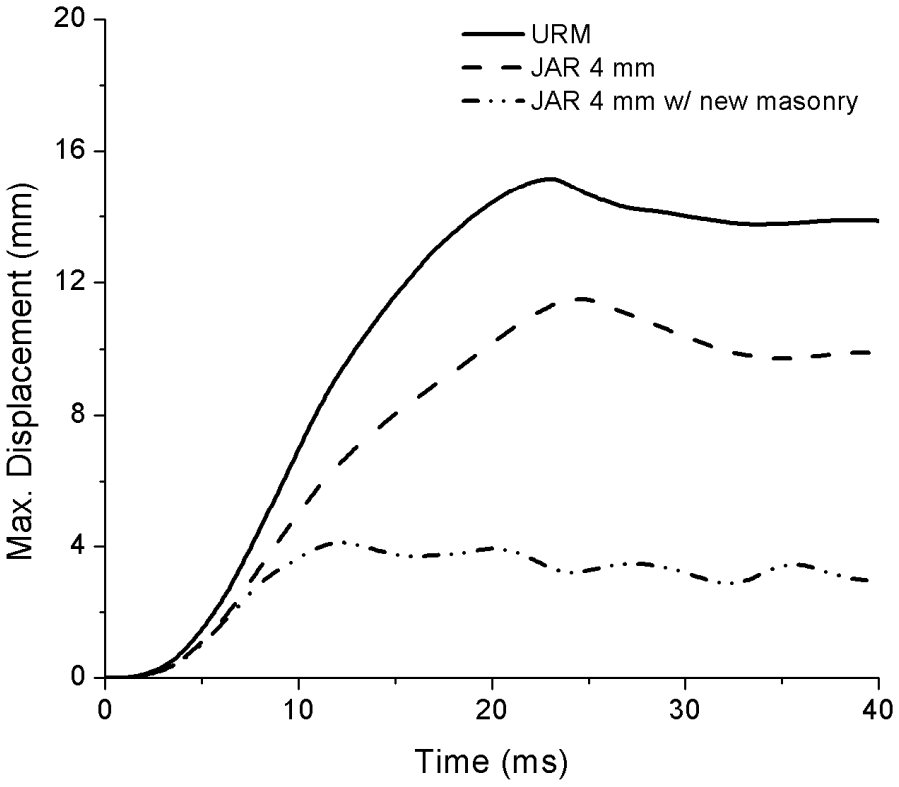

Figure 19: Influence of the compressive strength of masonry in the reinforced solutions.

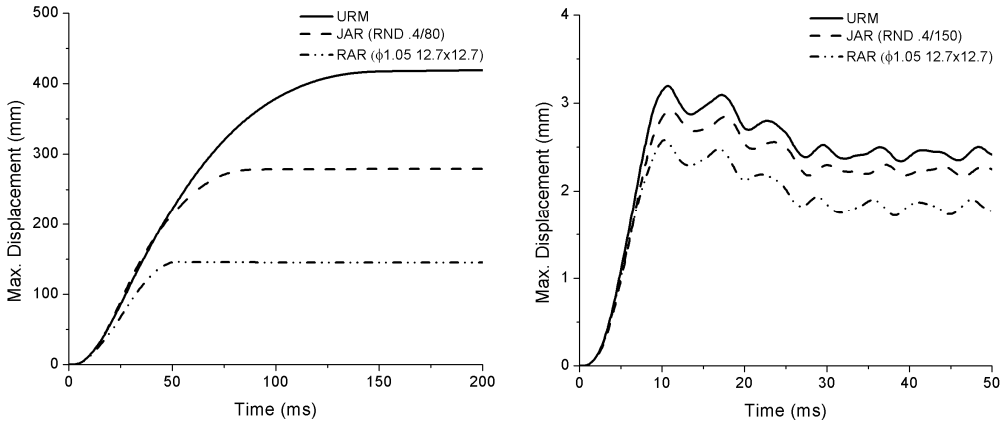

a) b)

Figure 20: Minimum reinforcement solutions: a) 140 mm thickness; b) 230 mm thickness.

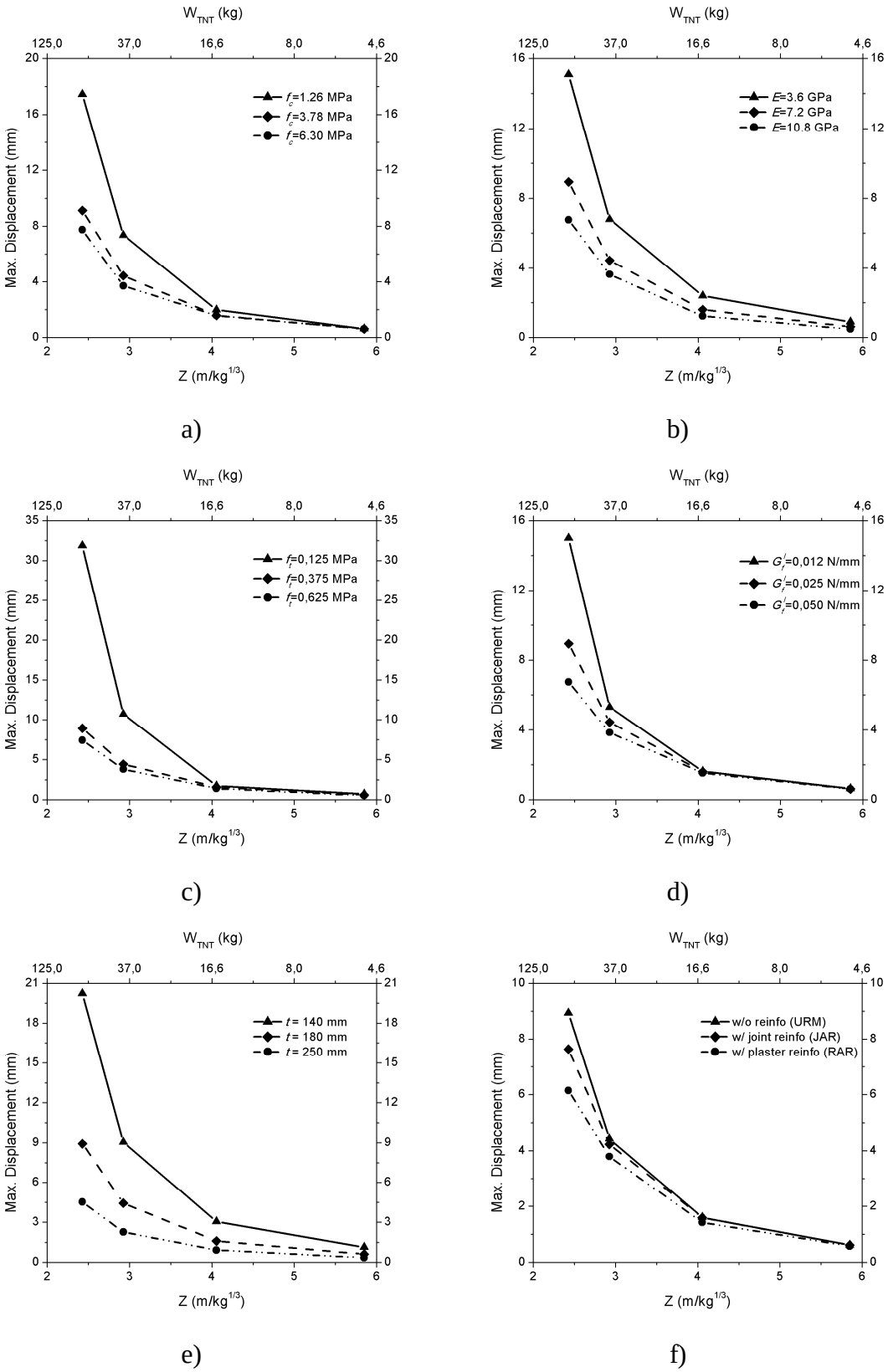

Figure 21 – Parametric study on the properties of infill walls subjected to blast loading: a) compressive strength; b) Young's modulus; c) tensile strength; d) mode-I fracture energy; e) thickness of the wall; f) reinforcement solution.

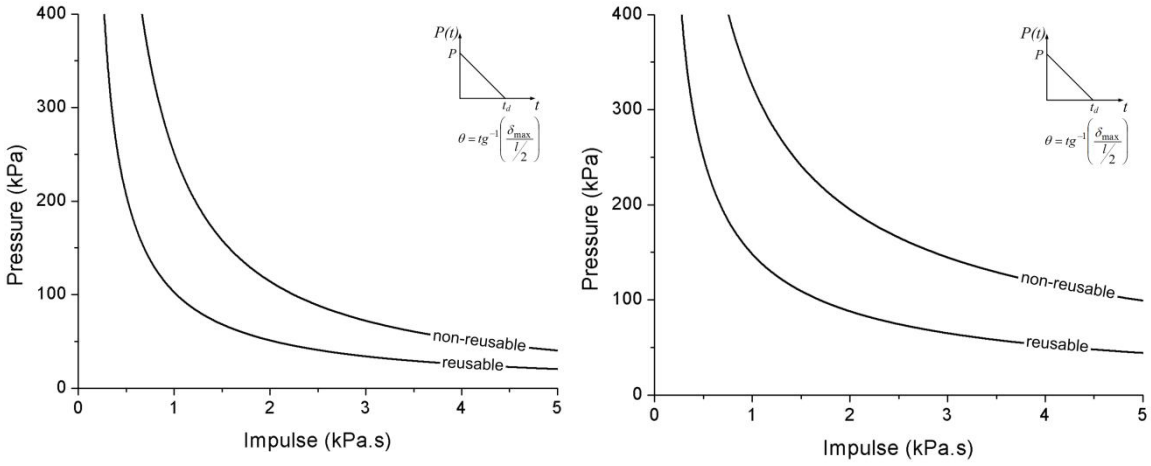

a) b)

Figure 22: P-I diagram for unreinforced masonry infill panel: a) 180 mm; b) 230 mm.

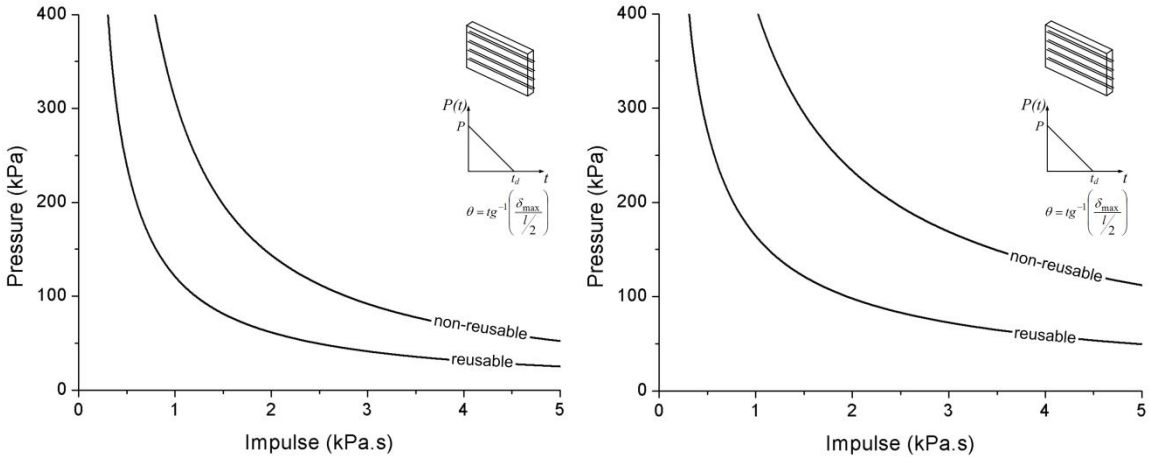

a) b)

Figure 23: P-I diagram for masonry infill panel with minimum bed joint reinforcement: a) 180 mm; b) 230 mm.

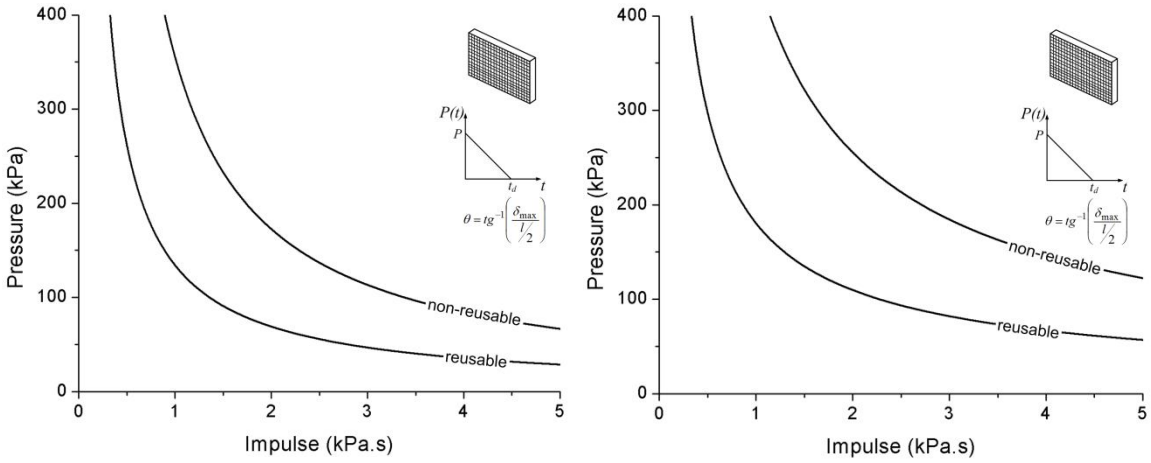

a) b)

Figure 24: P-I diagram for masonry infill panel with minimum grid reinforcement in the plaster: a) 180 mm; b) 230 mm.

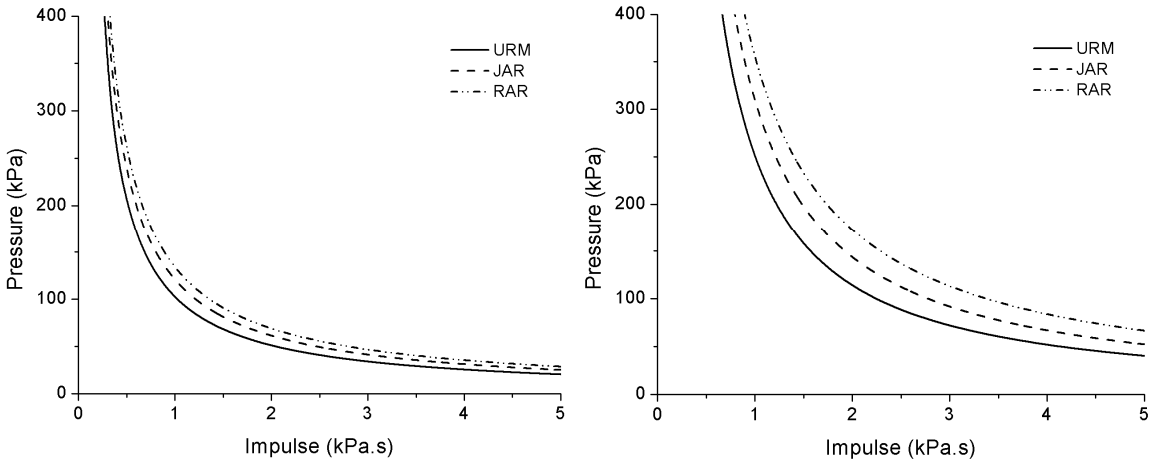

a) b)

Figure 25: P-I diagrams comparing three solutions for 180 mm: a) reusable stage; b) non-reusable stage.

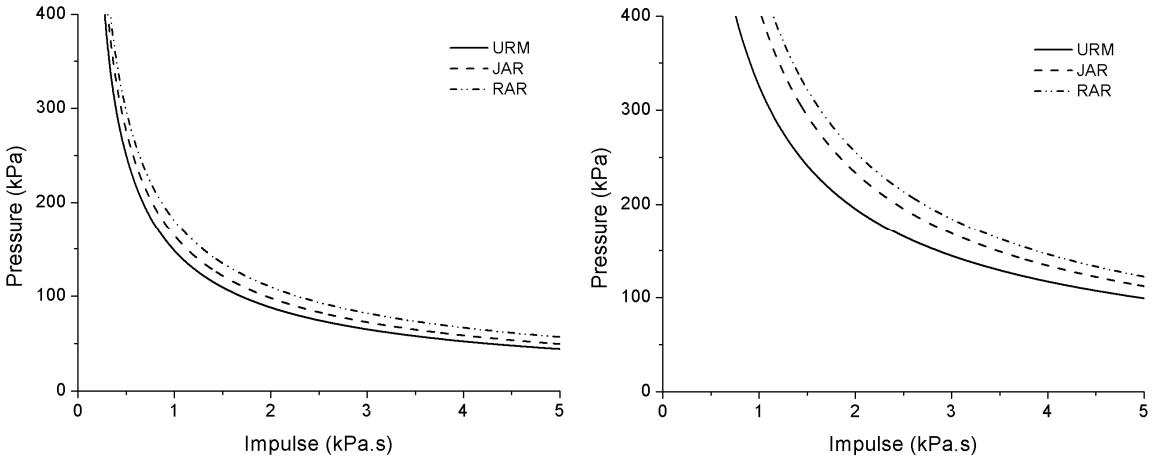

a) b)

Figure 26: P-I diagrams comparing three solutions for 230 mm: a) reusable stage; b) non-reusable stage.